

Jet entrainment: from the viscous superlayer to the turbulent core region

MAARTEN van REEUWIJK^{1†}
and
MARKUS HOLZNER²

¹Department of Civil and Environmental Engineering, Imperial College London, London, UK

²Institute of Environmental Engineering, ETH Zurich, Switzerland

(Received 3 April 2013)

We report on conditional statistics of turbulent entrainment in a temporal plane jet at $Re = 5000$ along enstrophy isosurfaces. The data is obtained by direct numerical simulation and the statistics span 24 orders of magnitude in the enstrophy threshold, ranging from essentially irrotational fluid outside the jet to the turbulent core region at the jet centre. We use two independent estimators for the local entrainment velocity v_n based on the enstrophy budget and develop a theoretical model that describes the expected behaviour inside the viscous superlayer. The model is in reasonably good agreement with the data and predicts that viscous transport has magnitude $2v_n$ and viscous dissipation $-v_n$. Although v_n is similar in magnitude to the Kolmogorov velocity u_η , its value is not independent of the threshold. Contrarily, the product between v_n and surface area S of the viscous superlayer, the *entrainment flux*, is independent of threshold implying that the local transport velocity and surface area adjust concertedly to the imposed global rate at the fringes of the turbulent layer. We divide the flow into a (i) viscous superlayer in which the transmission of enstrophy is dominated by viscous effects; (ii) a turbulent core region which is dominated by inertial production, viscous transport and dissipation; and (iii) an intermediate region that connects the two. The average distance between the core region and the viscous superlayer is about 10 Kolmogorov length scales, indicating that intense turbulent flow regions and viscosity-dominated regions are in close proximity.

1. Introduction

Turbulent entrainment is the incorporation of ambient fluid at the boundary of turbulent flows such as free shear flows or at the free stream edge of turbulent boundary layers. It is an important process in a variety of engineering and geophysical flows controlling the turbulent transfer of mass, heat and momentum (Pope 2000; Stull 1998; Thorpe 2005). A relevant, yet unresolved issue that has received renewed interest in recent years is the connection between processes that are associated with the large scale organization of the flow and processes that occur at the scale of the smallest eddies (e.g. Westerweel *et al.* 2005; Da Silva & Taveira 2010; Hunt *et al.* 2011; Philip & Marusic 2012; Wolf *et al.* 2012).

The integral rate at which ambient fluid is incorporated into the turbulent flow is independent of the small scale details of the flow, i.e. it does not depend on the viscosity or the energy dissipation mechanism. The common entrainment assumption is that the entrainment velocity u_e is proportional to the typical velocity \hat{u} inside the turbulent

† Email address for correspondence: m.vanreeuwijk@imperial.ac.uk

zone (Morton *et al.* 1956; Turner 1986), usually the centreline velocity. The entrainment coefficient $\alpha = u_e/\hat{u}$ is typically $O(0.1)$, but the value is far from universal and depends on the choice of the typical length scale b , the assumed shape of the velocity profile and can also depend on the initial conditions (e.g. Redford *et al.* 2012).

Conversely, Corrsin emphasised a *local* perspective and suggested that the turbulence boundary is demarcated by a very thin viscosity-dominated laminar superlayer, whose local propagation velocity v_n towards the non-turbulent region is determined by two parameters: the kinematic viscosity ν and the rate of dissipation of kinetic energy ε (Corrsin & Kistler 1955). Consequently, $v_n \propto u_\eta$ where u_η is the Kolmogorov velocity scale. The ratio of local entrainment velocity v_n to global (bulk) entrainment velocity u_e is given by

$$\frac{v_n}{u_e} \propto \frac{u_\eta}{\hat{u}} = \text{Re}^{-1/4}, \quad (1.1)$$

and the Reynolds number dependence begs the question in which way the two views - local and global - are consistent. The dependence on Re seems to imply that both surface area and viscous diffusion adjust to the imposed global rate such that the small scale details of how the vorticity is transferred are somehow forgotten across interactions of eddies with a large hierarchy of sizes (Townsend 1976). By denoting the integral entrainment flux as Q_e , the global perspective suggests that $Q_e = u_e A$, where A is the surface area based on the average distance of the turbulence interface to the core of the turbulent zone. From the local perspective $Q_e = v_n S$ where S is the total surface area of the contorted turbulence boundary. Equating the two expressions for Q_e results in $u_e/v_n = S/A$ and therefore

$$\frac{S}{A} \propto \text{Re}^{1/4}. \quad (1.2)$$

This means that S must be large to compensate a slow viscous transfer of vorticity and to cancel out the viscosity dependence (e.g. Tritton 1988; Sreenivasan *et al.* 1989).

Probably the simplest setting where turbulence propagates into non-turbulent fluid is the case without any mean flow, which can be realized via oscillating grid experiments, e.g. Holzner *et al.* (2007, 2008); Holzner & Luethi (2011). The results obtained in such a flow showed evidence for the presence of a laminar superlayer at the boundary of turbulent flow regions. In particular, the analysis supported that S is indeed given by a strongly convoluted surface and accounts for a large entrainment flux with a small characteristic velocity comparable to the Kolmogorov velocity (Holzner & Luethi 2011). A similar picture, i.e. $v_n \sim u_\eta$, recently emerged from the experiments in a round jet of Wolf *et al.* (2012). In all the experiments and simulations, the probability density functions (PDFs) of the entrainment velocity indicated that there is a large distribution in the actual entrainment velocity. In this context the term laminar superlayer is unfortunate as it suggests that the flow is layered without notable fluctuations. Therefore, this layer will be termed the *viscous* superlayer (VSL) in the remainder of the paper.

A somewhat different view emerges from direct numerical simulations of plane jets (Da Silva & Pereira 2008; Da Silva & Taveira 2010; Taveira & Da Silva 2013), a plane wake (Bisset *et al.* 2002) and experiments in a round jet (Westerweel *et al.* 2005, 2009), which focused on properties of the turbulent/nonturbulent interface (TNTI). The TNTI seemed to be thicker than the VSL predicted by Corrsin; that is, the thickness of the TNTI was found comparable to the Taylor length scale λ , rather than the Kolmogorov length scale η , although it was conjectured that the VSL may be contained inside the TNTI region Bisset *et al.* (2002). Also, the physical picture promoted differs from the one proposed by Corrsin in that it suggests that turbulence propagates mostly

via transmission of turbulent (i.e. Reynolds type) shear stresses (Westerweel *et al.* 2005, 2009), whereas it is the action of viscous shear forces in Corrsin’s theory.

One possible explanation for these differences in layer properties is the method by which the interface between the nonturbulent and turbulent fluid is identified. The interface is usually obtained by applying a threshold to a scalar field such as enstrophy (Bisset *et al.* 2002; Holzner *et al.* 2007; Da Silva & Pereira 2008) or a high Schmidt number dye (Westerweel *et al.* 2005). By construction, this interface is artificial because the transition between turbulent and nonturbulent fluid must occur smoothly over a finite region. The assumption is that the results are insensitive to the precise value of the threshold, and papers tend to provide anecdotal evidence that this is the case. For example, the fact that the interface is sharp is commonly used as an argument for level independence of the qualitative findings, as long as the thresholds lies within an interval where the gradient is sharp e.g. (Bisset *et al.* 2002). In addition, in experiments and even in numerical data sets it is often difficult to vary thresholds over a span of several decades because of experimental (e.g. Westerweel *et al.* 2005; Holzner *et al.* 2007) or numerical (e.g. Bisset *et al.* 2002) noise.

The aim of this paper is to perform a systematic study of the effect on the threshold value on the entrainment velocity and related statistics. Our analysis supports the existence of a VSL over a large range of thresholds (~ 20 decades), with a smooth transition to the turbulent core region. The study provides insight into how the local and global turbulent entrainment are connected to each other and what it implies for the geometry of the bounding surface. We find that the VSL is a nearly one-dimensional layer with low surface curvature and both its area and viscous transport velocity adjust to the imposed rate so that the entrainment flux is independent of threshold. We perform simulations of a temporal jet at $Re = 5000$ which has the advantage that it is well-documented (Da Silva & Pereira 2008), is a generic shear flow and is attractive from the viewpoint that this flow has two homogeneous directions. The present paper starts out with a theoretical framework that describe the properties of the local entrainment velocity from a local and a integral perspective. Predictions are made based on a simple model and tested against the simulation data. Next, properties of the geometry and surface area of the VSL are presented. In the final section the results are brought in context with previous work and possible non-universality issues are discussed. In a companion paper the influence of mean shear and Reynolds number are analysed.

2. Theory

This section revisits the determination of the local entrainment velocity based on enstrophy budgets from a local perspective and complements it with an integral approach to the problem. Thereafter a simplified model is set out with predictions for the enstrophy transport across the VSL.

2.1. Local entrainment velocity: classical approach

We separate between turbulent and non-turbulent flow regions by using a threshold on the enstrophy $\omega^2 \equiv \omega_i \omega_i$, where ω_i is a component of vorticity. This defines a bounding surface separating the two regions. In a Lagrangian frame moving with the iso-enstrophy surface the isovalue will by definition remain constant and this property can be used to derive an expression for the propagation velocity (Holzner & Luethi 2011). We write the velocity of an isosurface element, \mathbf{v} , as a sum of fluid velocity, \mathbf{u} , and velocity of the area element relative to the fluid, \mathbf{V} , that is, $\mathbf{v} = \mathbf{u} + \mathbf{V}$. The total change of ω^2 in a frame

of reference moving with an enstrophy isosurface element is then given by

$$\frac{d\omega^2}{dt} = \frac{\partial\omega^2}{\partial t} + \mathbf{v} \cdot \nabla\omega^2 = \frac{D\omega^2}{Dt} + \mathbf{V} \cdot \nabla\omega^2 = 0, \quad (2.1)$$

where the lower case d/dt is the total derivative following a surface element, and the upper case D/Dt is the material derivative which follows a fluid element. By defining a surface normal as $\hat{\mathbf{n}} = \nabla\omega^2/|\nabla\omega^2|$ and the normal relative velocity component $\hat{v}_n = \mathbf{V} \cdot \hat{\mathbf{n}}$, we obtain

$$\hat{v}_n = -\frac{1}{|\nabla\omega^2|} \frac{D\omega^2}{Dt}. \quad (2.2)$$

Substituting the enstrophy balance equation

$$\frac{D}{Dt} \left(\frac{\omega^2}{2} \right) = \nu \nabla^2 \left(\frac{\omega^2}{2} \right) + \omega_i \omega_j s_{ij} - \nu \nabla\omega_i \cdot \nabla\omega_i \quad (2.3)$$

into (2.2) and averaging over the isosurface $\langle \cdot \rangle_S$, we obtain an expression for the average entrainment velocity v_n :

$$v_n \equiv \langle \hat{v}_n \rangle_S = v_L^{\mathcal{P}} + v_L^{\mathcal{D}} + v_L^{\mathcal{E}}, \quad (2.4)$$

where

$$v_L^{\mathcal{P}} = -\left\langle \frac{2\omega_i \omega_j s_{ij}}{|\nabla\omega^2|} \right\rangle_S, \quad v_L^{\mathcal{D}} = -\left\langle \frac{\nu \nabla^2 \omega^2}{|\nabla\omega^2|} \right\rangle_S, \quad v_L^{\mathcal{E}} = \left\langle \frac{2\nu \nabla\omega_i \cdot \nabla\omega_i}{|\nabla\omega^2|} \right\rangle_S.$$

Using the definition of $\hat{\mathbf{n}}$, the viscous term can be decomposed into a contribution due to curvature and normal transport through the following identity (Holzner & Luethi 2011):

$$\nabla\omega^2 = |\nabla\omega^2| \nabla \cdot \hat{\mathbf{n}} + \hat{\mathbf{n}} \cdot \nabla |\nabla\omega^2| \quad (2.5)$$

This identity will be used to quantify the role of curvature in §4.2.

2.2. Local entrainment velocity: integral approach

An alternative to the local approach described in § 2.1 is to integrate the enstrophy equation (2.3) over a time-dependent domain $D(t)$ which has boundary velocity \mathbf{v} and use the Reynolds transport theorem, resulting in

$$\begin{aligned} \frac{d}{dt} \int_D \frac{\omega^2}{2} dV + \oint_{\partial D} (\mathbf{u} - \mathbf{v}) \cdot \hat{\mathbf{n}} \left(\frac{\omega^2}{2} \right) dS &= \nu \oint_{\partial D} \nabla \left(\frac{\omega^2}{2} \right) \cdot \hat{\mathbf{n}} dS \\ &+ \int_D \omega_i \omega_j s_{ij} dV - \nu \int_D \nabla\omega_i \cdot \nabla\omega_i dV. \end{aligned}$$

As the surface normal $\hat{\mathbf{n}}$ points into the turbulent region, the appropriate volume under consideration comprises the irrotational region. We can formalise this by defining a control volume $D = H(1 - \omega^2/\omega_0^2)$ where H is the Heaviside function and ω_0^2 is a enstrophy threshold. As ω^2 is then by definition constant on the surface ∂D , the equation above simplifies to

$$\begin{aligned} \oint_{\partial D} \mathbf{V} \cdot \hat{\mathbf{n}} dS &= \frac{2}{\omega_0^2} \left(\frac{d}{dt} \int_D \frac{\omega^2}{2} dV - \nu \oint_{\partial D} \nabla \left(\frac{\omega^2}{2} \right) \cdot \hat{\mathbf{n}} dS \right. \\ &\quad \left. - \int_D \omega_i \omega_j s_{ij} dV + \nu \int_D \nabla\omega_i \cdot \nabla\omega_i dV \right). \end{aligned} \quad (2.6)$$

Defining[†]

$$\frac{dV}{dt} = \oint_{\partial D} \mathbf{V} \cdot \hat{\mathbf{n}} dS \equiv v_n S, \quad S = \oint_{\partial D} dS, \quad V = \int_D dV, \quad (2.7)$$

and introducing an average over the volume $\langle \cdot \rangle_V$, (2.6) can be rewritten as

$$\left(1 - \frac{\langle \omega^2 \rangle_V}{\omega_0^2}\right) v_n = -\frac{2\nu}{\omega_0^2} \left\langle \frac{d\omega^2}{dn} \right\rangle_S + \frac{2V}{S\omega_0^2} \left(\frac{d}{dt} \frac{\langle \omega^2 \rangle_V}{2} - \langle \omega_i \omega_j s_{ij} \rangle_V + \nu \langle \nabla \omega_i \cdot \nabla \omega_i \rangle_V \right).$$

Now, because D spans the entire nonturbulent region, it is expected that $\langle \omega^2 \rangle_V / \omega_0^2 \ll 1$, and therefore

$$v_n \approx v_I^{\mathcal{D}} + v_I^{\mathcal{T}} + v_I^{\mathcal{P}} + v_I^{\mathcal{E}}, \quad (2.8)$$

where

$$\begin{aligned} v_I^{\mathcal{D}} &= -\frac{2\nu}{\omega_0^2} \left\langle \frac{d\omega^2}{dn} \right\rangle_S, & v_I^{\mathcal{T}} &= \frac{2V}{S\omega_0^2} \frac{d}{dt} \frac{\langle \omega^2 \rangle_V}{2}, \\ v_I^{\mathcal{P}} &= -\frac{2V}{S\omega_0^2} \langle \omega_i \omega_j s_{ij} \rangle_V, & v_I^{\mathcal{E}} &= \frac{2V}{S\omega_0^2} \nu \langle \nabla \omega_i \cdot \nabla \omega_i \rangle_V. \end{aligned}$$

2.3. A model for enstrophy transport in the viscous superlayer

In the VSL, the evolution of enstrophy is governed by molecular processes (Corrsin & Kistler 1955; Holzner & Luethi 2011), i.e. $|v^{\mathcal{P}}/v_n| \ll 1$. Assuming that the local curvature is small on average and multiplying by $d\omega^2/dn$, Eq. (2.4) then becomes

$$\frac{d\omega^2}{dn} v_n + 2\nu\omega \frac{d^2\omega}{dn^2} = 2\omega \frac{d}{dn} \left(v_n \omega + \nu \frac{d\omega}{dn} \right) = 0. \quad (2.9)$$

Integrating this expression and using that at $n = -\infty$, both $\omega = 0$ and $d\omega/dn = 0$, we obtain

$$v_n \omega + \nu \frac{d\omega}{dn} = 0. \quad (2.10)$$

Assuming that v_n is constant in the VSL, the square of the solution to (2.10) is

$$\frac{\omega^2}{\omega_r^2} = \exp \left(\frac{-2v_n(n - n_r)}{\nu} \right), \quad (2.11)$$

where $\omega_r^2 = \omega(n_r)$ is a reference value for enstrophy. Hence, the enstrophy is expected to drop off exponentially in the VSL, provided that v_n is constant (see §4.2).

The model solution (2.11) can be used to predict the magnitude of the enstrophy transport terms. For the local approach we expect

$$\begin{aligned} v_L^{\mathcal{D}} &\approx -\nu \frac{d^2\omega^2}{dn^2} \left(\frac{d\omega^2}{dn} \right)^{-1} = 2v_n, \\ v_L^{\mathcal{E}} &\approx 2\nu \left(\frac{d\omega}{dn} \right)^2 \left(\frac{d\omega^2}{dn} \right)^{-1} = -v_n. \end{aligned}$$

[†] The first equation holds because $\oint \mathbf{u} \cdot \hat{\mathbf{n}} dS = 0$ for an incompressible fluid.

Entirely consistently, we expect for the integral approach that

$$\begin{aligned} v_I^{\mathcal{D}} &\approx \frac{\nu}{\omega^2} \frac{d\omega^2}{dn} = 2v_n, \\ v_L^{\mathcal{E}} &\approx \frac{2\nu}{\omega^2} \int_{-\infty}^n \left(\frac{d\omega}{dn} \right)^2 dn = -v_n. \end{aligned}$$

3. Simulations

The start situation for a temporal plane jet is a fluid layer that is quiescent except for a thin region $-b_0 < y < b_0$ in which the streamwise velocity u is nonzero, and is homogeneous in the two other directions x and z . Here, b_0 is the initial jet width. It follows from continuity that the volume flux $q = \int u dy$ remains constant for this flow throughout the jet's transition to turbulence and subsequent growth due to turbulent entrainment. Assuming that the Reynolds number $Re \gg 1$, the only relevant parameters are the initial volume flux q_0 and time t which suggests self-similar behaviour, with the jet halfwidth b and centreline velocity \hat{u} scaling as $b \propto \sqrt{q_0 t}$ and $\hat{u} \propto \sqrt{q_0/t}$, respectively.

The simulation domain is a cuboid of size $24b_0 \times 36b_0 \times 24b_0$, which is three times larger in all directions than the domain used in Da Silva & Pereira (2008). The larger domain facilitates much longer simulations, thereby allowing not only the first moments but also the turbulence to reach an equilibrium and has the added advantage of improved statistics because of the larger area spanned by the two homogeneous directions. The simulation considered here is for $Re \equiv 2q_0/\nu = 5000$. The resolution of the simulation is $1024 \times 1536 \times 1024$ which is sufficient to ensure that all active length scales in the turbulence are fully resolved. We define a reference time-scale $t^* = b_0^2/q_0$ and simulate for $300t^*$. All statistics before $t/t^* = 150$ are discarded to ensure that the turbulence has time to reach a dynamic equilibrium.

Following Da Silva & Métais (2002); Da Silva & Pereira (2008), we use the initial condition

$$u(y, 0) = \frac{U_0}{2} \left[1 + \tanh \left(\frac{b_0 - |y|}{2\theta_0} \right) \right], \quad (3.1)$$

where U_0 is chosen such that $\int u dy = q_0$. The initial condition is then seeded with uniform random noise of such amplitude that the enstrophy level due to noise is 8 percent of the maximum average enstrophy level [which is $(U_0/(4\theta_0))^2$]. The code used for direct numerical simulation is based on fully conservative second order finite difference operators in space (Verstappen & Veldman 2003) and uses an adaptive second-order Adams-Bashforth time integration scheme. More details can be found in van Reeuwijk *et al.* (2008).

As the statistics shown in the next section depend heavily on budgets for the enstrophy, special care is taken to ensure that the budgets are calculated consistently with the numerics used. To achieve this, a mimetic (Hyman & Shashkov 1997; van Reeuwijk 2011) **curl** operator is defined such that it satisfies the identity $\nabla \times \nabla p = 0$ up to machine precision, where p denotes pressure. In order to ensure calculation fully compatible with the numerical method, we do not manually discretise (2.3), but instead make use of the following identities

$$\omega_i \omega_j s_{ij} = (\mathbf{u} \cdot \nabla) \frac{\omega^2}{2} - \omega \cdot (\nabla \times (\mathbf{u} \cdot \nabla) \mathbf{u}), \quad (3.2)$$

$$\nu \nabla \omega_i \cdot \nabla \omega_i = \nu \nabla^2 \left(\frac{\omega^2}{2} \right) - \nu \omega \cdot (\nabla \times \nabla^2 \mathbf{u}), \quad (3.3)$$

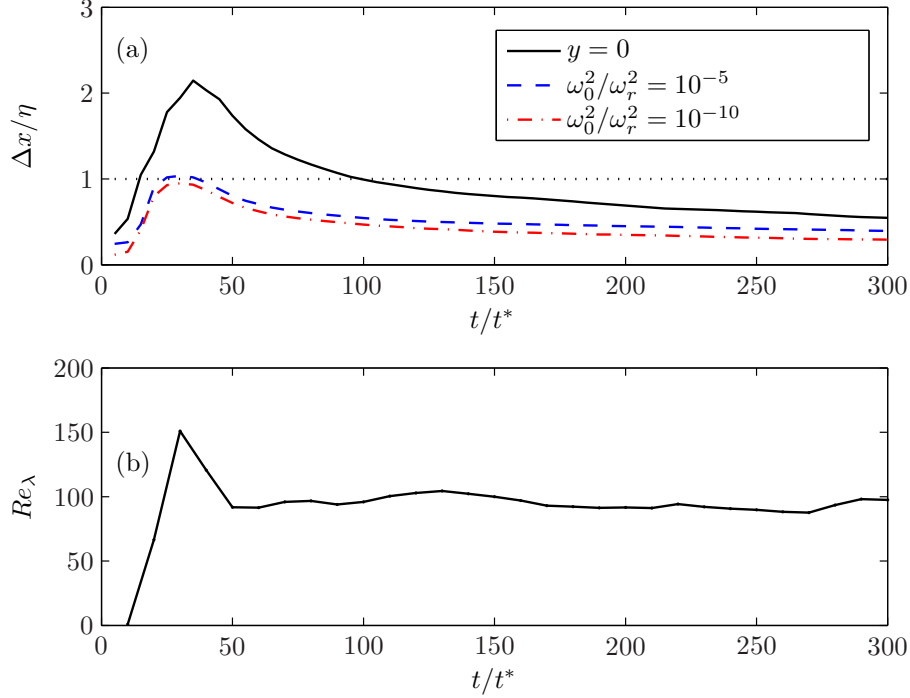


FIGURE 1. (a) Δx normalised by the Kolmogorov scale η ; (b) Re_λ against time.

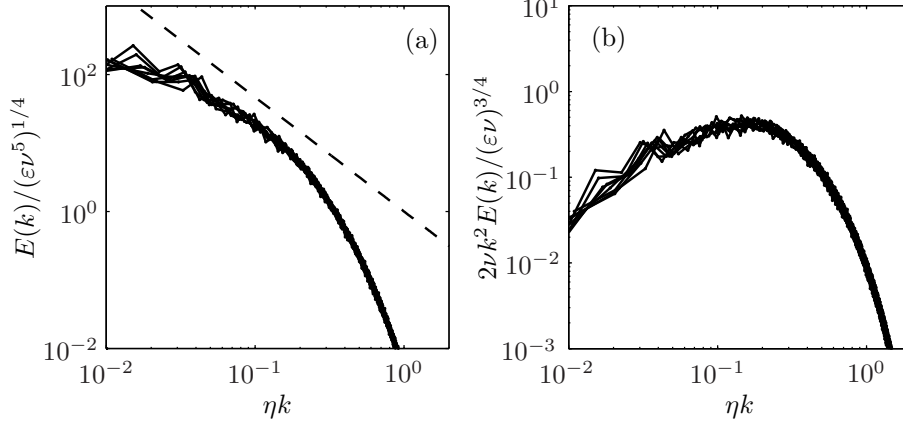
which are then also enforced on the discrete level. Taking (3.3) as an example, one can calculate the first term on the right hand side directly by using the routine for scalar diffusion on $\omega^2/2$; the second term can be calculated by taking the discrete curl of the viscous term in the momentum equation, and then taking the scalar product of the result with the vorticity components.

As the temporal jet has a nonzero mean velocity in the x -direction, it is important to ensure that the identity $\oint \mathbf{u} \cdot \hat{\mathbf{n}} dS = 0$ is also satisfied on the discrete level. Indeed, this identity was used explicitly to derive (2.7). This can only be achieved if the thresholding algorithm identifies entire cells to be either inside or outside the turbulent region. Indeed, we found that if we used bilinear interpolation to construct an isosurface - which is in principle a better representation - the various interpolations required could lead to very significant deviations in the calculated entrainment velocity.

4. Results

4.1. Bulk flow properties

Fig. 1(a) demonstrates that the grid resolution is appropriate for the problem under consideration. Shown is the grid spacing normalised by the Kolmogorov length scale $\eta = (\nu^3/\varepsilon)^{1/4}$ based on the centreline dissipation rate $\varepsilon(t) \equiv \overline{\varepsilon}(y=0, t)$. The overbar denotes averaging over the two homogeneous directions and over 10 t^* . The dissipation rate has its maximum at $y=0$ and dissipation rates will be much lower at the jet boundary, which implies that the simulation is even better resolved there (dashed and dash-dotted lines). As can be seen, the simulation becomes better resolved in time because $\eta \propto \sqrt{t}$, which can be inferred by using that $\varepsilon \propto \hat{u}^3/b$, as is confirmed in Fig. 3(d). Fig. 1(b) shows the evolution of the Taylor Reynolds number, defined as $Re_\lambda = (20/3)e^2/\sqrt{\nu\varepsilon}$ (e.g. Tennekes

FIGURE 2. Energy density (left) and dissipation spectra (right) at $y = 0$.

& Lumley 1972), where $e(t) \equiv \bar{e}(y = 0, t)$ is the turbulent kinetic energy. As judged from Re_λ , the turbulence reaches an equilibrium value of about $Re_\lambda \approx 100$ after $t/t^* = 50$.

Energy density spectra for the plane $y = 0$, averaged over shells of wave number $\sqrt{k_x^2 + k_z^2}$ and a time interval of $10t^*$ are shown in Figure 2. The spectra indicate that there is a range of active scales and that there is a separation of scales as is evident from the formation of a $k^{-5/3}$ spectrum (left) and the peak in the dissipation spectrum (right). Sixteen spectra are shown for $t/t^* > 150$ and the collapse clearly demonstrates the self-similarity of the flow under consideration; even though the spectra change in time, the normalisation with η and ε cause a full collapse of the data.

As the velocity profile is symmetric around $y = 0$, the jet half-width b was inferred from the average of the values of b for which $\bar{u}(b, t) = \hat{u}(t)/2$ and $\bar{u}(-b, t) = \hat{u}(t)/2$. For all profiles shown, use has been made of the symmetry (or anti-symmetry) in the profile to further improve the statistical accuracy. Shown in Fig. 3(a) is the scaling of b^2 with time, which as expected from dimensional arguments is linear; the red dashed line is a linear fit. The normalised mean velocity \bar{u} and momentum flux $\overline{v'u'}$ are shown in Fig 3(b,c). These profiles were scaled and then further averaged over four contiguous time-intervals (an effective average over $40 t^*$). The profiles are convincingly self-similar. Self-similarity of turbulent quantities is demonstrated in Figs 3(d-f). As discussed earlier, the balance between turbulence production and dissipation suggests that $\bar{\varepsilon} \propto \hat{u}^3/b$ (Fig. 3(f)), which in turn implies that $\eta \propto b$ (Fig. 3(d)). The profiles for the turbulence kinetic energy (TKE) $\bar{\varepsilon}$ and the dissipation rate $\bar{\varepsilon}$ (Figs 3(e, f)) show once more a reasonably good collapse, with $\bar{\varepsilon}$ peaking at $y/b \approx 1$ (where shear-production is maximal) and the dissipation rate $\bar{\varepsilon}$ peaking at the centreline. Consistent with recent work by Redford *et al.* (2012), we observed quite substantial variations in the growth rate of b between different simulations despite a convincing self-similar behaviour in all of them. This points to non-universal self-similar behaviour (Redford *et al.* 2012).

4.2. Entrainment velocity and budgets

A cross-section of the enstrophy field at constant z is shown in Fig. 4, together with a number of enstrophy isolines. Bisset *et al.* (2002); Da Silva & Pereira (2008) use a threshold value $\omega_0 = 0.7U_0/(2b_0)$ which corresponds with $\omega_0^2/\omega_r^2 \approx 0.1$, where we have defined a reference enstrophy level $\omega_r^2 = U_0^2/b_0^2$. At this enstrophy level, the turbulent/nonturbulent interface is highly contorted and has 'holes'. Also shown are two enstrophy thresholds that are much lower, namely $\omega_0^2/\omega_r^2 = 10^{-12}$ and 10^{-6} . What is striking is that these

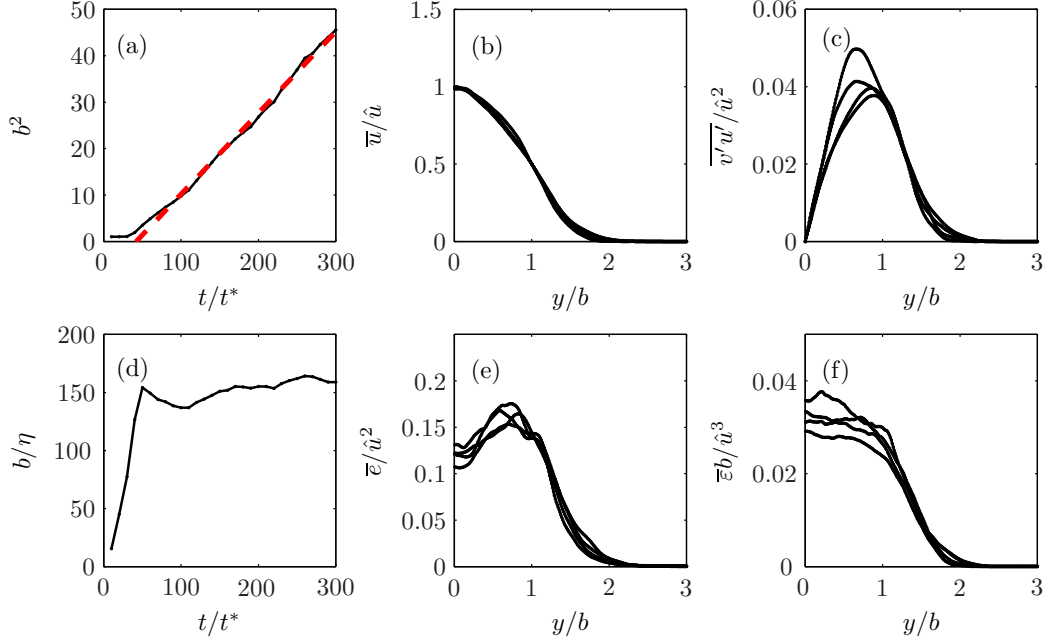


FIGURE 3. Self-similarity of the temporal plane jet. (a) dependence of b^2 on time; (b) average velocity \bar{u} ; (c) turbulent momentum flux $\overline{v'u'}$; (d) dependence of b/η on time. (e) kinetic energy $\bar{\epsilon}$; and (f) the dissipation rate $\bar{\epsilon}$.

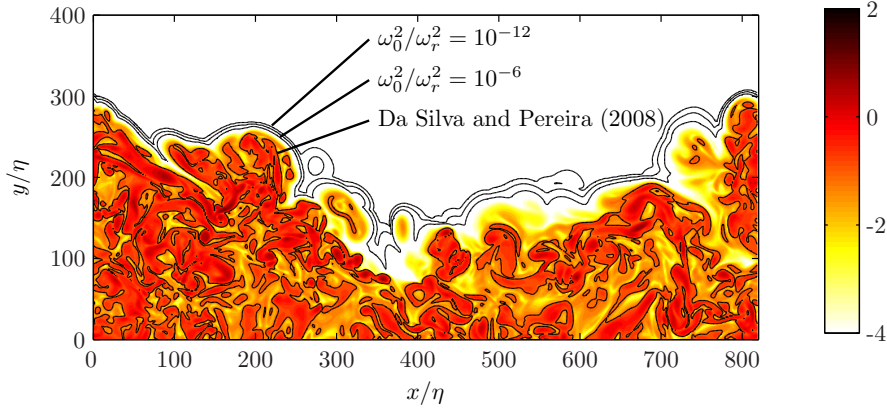


FIGURE 4. A field in cross-section showing $^{10} \log(\omega^2/\omega_r^2)$ at $t/t^* = 150$. Also shown are various isocontours of enstrophy.

low enstrophy levels are in close proximity to the high enstrophy regions, indicating a very quick drop-off of enstrophy levels near the jet edge. At these low threshold values, there are no more holes visible[†] in the figure, and although the surface remains contorted because of the large scale vortices distorting the flow, the enstrophy isosurfaces appear to form nearly one-dimensional layers with relatively small curvature.

The instantaneous budgets of enstrophy were calculated for the entire 3-D field every $5 t^*$ and then used to calculate the terms in (2.4), (2.8) for 37 thresholds in the range

[†] Note that what may appear as holes on the Fig. (i.e. in 2D) are fluid portions that are connected in 3D to the outer irrotational region.

$\omega_0^2/\omega_r^2 \in [10^{-24}, 10^0]$. Simultaneously, the volume V was recorded for each of the threshold values, which enabled an independent calculation of the propagation velocity v_n using (2.7). Shown is the data for $t/t^* > 150$.

The terms comprising the local entrainment velocity v_L (2.4) normalised by the directly measured volume-based entrainment velocity v_n are presented in Fig. 5(a). For $\omega_0^2/\omega_r^2 < 10^{-5}$, the predicted propagation velocity v_L (squares) excellently matches the actual propagation velocity. The poor predictions for $\omega_0^2/\omega_r^2 > 10^{-5}$ are related to an insufficient temporal sampling frequency creating large errors in the calculation of $v_n \approx \delta V/\delta t$ (Eq. 2.7) at high enstrophy levels.

Consistent with earlier findings, the inviscid contribution $v_L^{\mathcal{P}}$ (circles) does not play a role in the VSL (Holzner & Luethi 2011). For $\omega_0^2/\omega_r^2 > 10^{-5}$, the inviscid terms become dominant very rapidly, and note that the enstrophy level employed by Da Silva & Pereira (2008) and others is $\omega_0^2/\omega_r^2 = 10^{-1}$. Also shown in Fig. 5(a) are the theoretical predictions from §2.3, namely $v_L^{\mathcal{D}} = 2v_n$ and $v_L^{\mathcal{E}} = -v_n$ (both displayed by dotted lines). The predictions are in good agreement, although the observed magnitudes of $v_n^{\mathcal{E}}$ (downward triangles) and $v_n^{\mathcal{D}}$ (upward triangles) are a bit larger. The plots of v_L reveal a slight decrease at lower threshold levels, indicating that there is a small systematic error in the calculation of v_L .

Fig. 5(b) shows an identical calculation but using the integral approach outlined in §2.2. As for v_L , the propagation velocity v_I is in excellent agreement with v_n for $\omega_0^2 < \omega_r^2$. The temporal and inviscid contributions, $v_I^{\mathcal{T}}$ (diamonds) and $v_I^{\mathcal{P}}$ (circles) respectively, are negligible and the propagation of the enstrophy isosurface in the VSL is caused by viscous effects. It is noted that for this indicator, the contributions $v_I^{\mathcal{D}}$ and $v_I^{\mathcal{E}}$ seem to become independent of the threshold level below $\omega_0^2/\omega_r^2 < 10^{-5}$. Furthermore, v_I/v_n becomes constant for small threshold values, although the ratio is slightly smaller than 1.

One of the main assumptions made in the derivation of the theoretical model was that the curvature of the isosurface is small. The reasonably good agreement with the theoretical model in Fig. 4 supports this assumption but using Eq. 2.5 it can be validated explicitly. Figs 5(c,d) show the contribution to $v^{\mathcal{D}}$ by curvature (red crosses) and diffusive transport in the direction of the surface normal (blue triangles). For both v_L as v_I , the curvature term becomes negligible for $\omega_0^2/\omega_r^2 < 10^{-5}$. This provides confirmation that the theoretical model in §2.3 is a reasonable description of the processes governing the VSL.

Having established that both estimates of the local entrainment velocity v_L and v_I are in good agreement with the actual entrainment velocity v_n , we study the dependence of the entrainment velocity on the threshold value ω_0^2 . The bulk entrainment velocity is defined as $u_e = L^{-2}dV/dt$ where $L = 24b_0$, and is therefore related to v_n (Eq. 2.7) by $u_e = -(S/L^2)v_n$. In Fig. 6 we show the dependence of v_n , v_L and v_I on ω_0^2 .

There is a clear dependence of v_n on the enstrophy threshold when normalising by u_η [Fig. 6(a)]; isosurfaces for the very low enstrophy thresholds propagate faster than those with higher thresholds. Indeed, v_L is nearly twice as high at $\omega_0^2/\omega_r^2 = 10^{-24}$ than at $\omega_0^2/\omega_r^2 = 10^{-6}$. Hence, although v_n is of the same order of magnitude as u_η , the dependence on ω_0^2 suggests that it is not merely the viscosity ν and dissipation rate ε that determine the propagation velocity in the VSL. Another striking feature is that v_n becomes zero around $\omega_0^2/\omega_r^2 \approx 10^{-3}$ for the timespan under consideration and negative for $\omega_0^2/\omega_r^2 > 10^{-3}$. Hence, high enstrophy regions move towards the jet centre and the low enstrophy regions move outwards. This can be explained by using the relation between enstrophy and the dissipation rate which is valid for isotropic and homogeneous turbulence $\varepsilon = \nu \overline{\omega' \omega'}$. Using the self-similarity of ε it follows that $\overline{\omega' \omega'} \approx \hat{u}^3/(\nu b) \propto t^{-2}$. Hence,

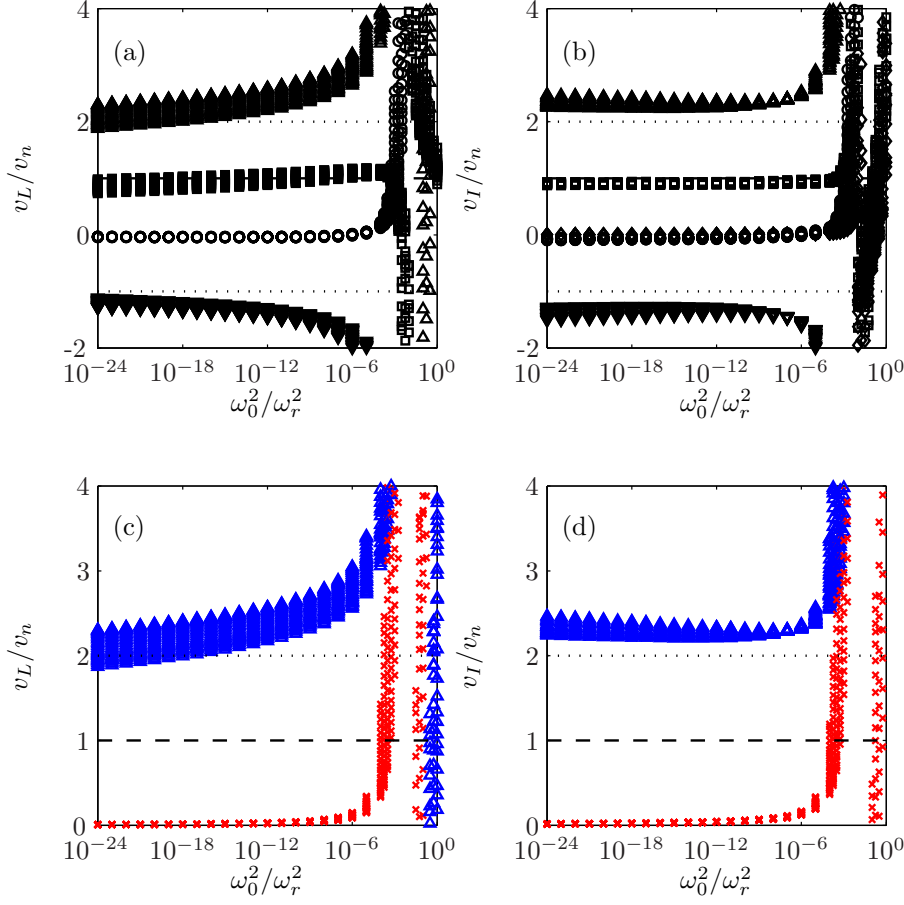


FIGURE 5. the local entrainment velocity decomposed into various contributions and normalised by the actual propagation velocity v_n . v^D [Δ], v^P [\circ], v^E [∇], v^D [\diamond], total [\square]. (a,c) v_L ; (b,d) v_I . Figs (c,d) show the decomposition of v^D in a contribution due to curvature (red crosses) and normal transport (blue triangles).

if one would assume that $\overline{\omega'\omega'}$ has a self-similar profile and pick a reference threshold ω_0^2 that is followed in time, it would be seen to move towards the jet core. This applies to enstrophy levels where turbulence is developed and v_n is positive. Towards the VSL, at low ω^2 levels, viscous transport is diffusing enstrophy outwards and v_n is negative. Note that the gradient of v_n over ω^2 in Fig. 6(a) is always negative meaning that the enstrophy profile is flattening over time.

Fig. 6(b) shows the bulk entrainment velocity u_e normalised by the centreline velocity amplitude \hat{u} . The standard entrainment assumption (e.g. Turner 1986) is $u_e = \alpha \hat{u}$ and the ratio plotted is the entrainment coefficient α . As can be seen, α is much less dependent on $\omega_0^2 < \omega_r^2$ than v_n/u_η . If α were entirely independent of ω_0^2 , it would imply that the entrainment flux Q_e is constant; indeed, by using that $u_e = v_n S/L^2 = Q_e/L^2$ it would immediately follow that Q_e is constant if u_e is independent of ω_0^2 . Even though a small dependence on α is discernible, this result does indicate that to first order $S \propto v_n^{-1}$, and only if $v_n \propto u_\eta$ is independent of ω_0^2 do we expect that $S \propto Re^{1/4}$, independently of ω_0^2 , i.e. the classical view advocated by Corrsin.

Full independence of the entrainment velocity u_e of the enstrophy threshold ω_0^2 can

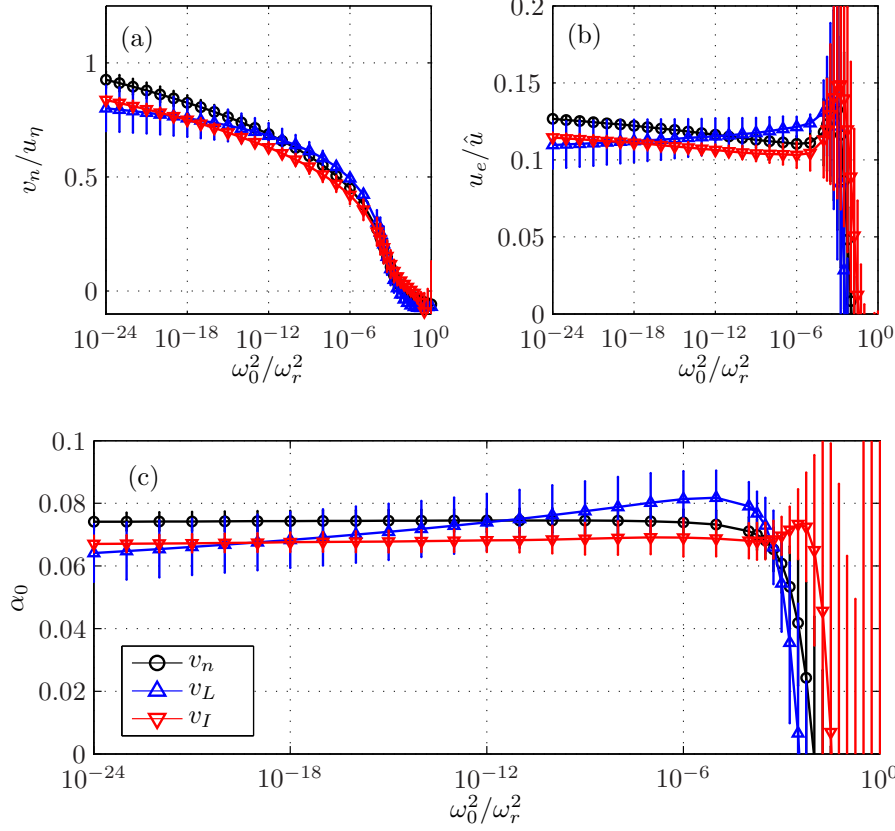


FIGURE 6. Entrainment velocities as a function of threshold. (a) v_n normalised by u_η . (b) u_e normalised by \hat{u} . (c) normalised entrainment coefficient α_0 .

be achieved by taking into account the position of the interface. Selfsimilarity implies that $\bar{u} = \hat{u}f(\xi)$, where f is the universal velocity profile and $\xi = y/b$ the selfsimilarity variable. The entrainment assumption is $u_{e0} = \alpha_0 \hat{u}$, where u_{e0} is defined as $u_{e0} \equiv db/dt$. As mentioned in §1, other definitions of b will result in different values for α . This is straightforward to see by fixing ξ at a value differing from unity. Indeed, for an alternative width $y = \xi b$, we obtain

$$u_e = \frac{dy}{dt} = \xi \frac{db}{dt} = \alpha_0 \xi \hat{u}, \quad (4.1)$$

indicating that the effective entrainment rate is $u_e/\hat{u} = \xi \alpha_0$. Hence, if there is a dependence of the average interface position $\langle y \rangle_S$ on the enstrophy isosurface this will create a trend in u_e . In Fig. 6(c), we have plotted $\alpha_0 = u_e/(\xi \hat{u})$, where $\xi = \langle y \rangle_S/b$. As can be seen, both u_n as u_I are constant as a function of the threshold value. There is a downward trend for u_L which is consistent with Figs 5(b) and 6(b), but as v_n is directly calculated from V , we consider this data to be more trustworthy.

There are two distinguishing enstrophy threshold values to consider at any time, namely (i) the enstrophy level at which $v_n = 0$ and (ii) the enstrophy level for which enstrophy production becomes negligible, diagnosed by the operational criterion $|v_n^P/v_n| < 0.05$. The former demarcates a threshold which separates expanding areas ($v_n < 0$) from shrinking areas ($v_n > 0$) and the latter demarcates the start of the VSL. These threshold levels are plotted as a function of time in Fig. 7 for v_L (solid lines) and v_I (dashed lines).

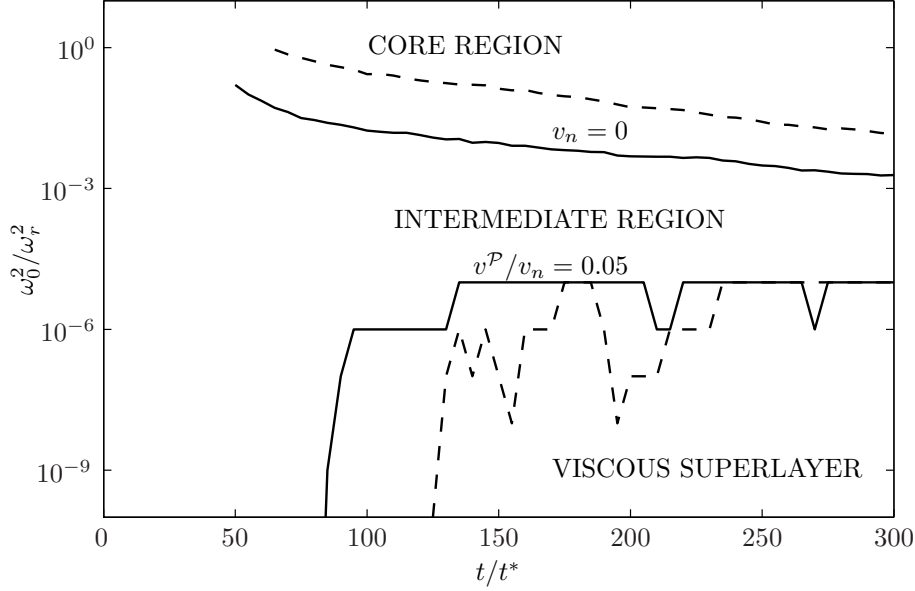


FIGURE 7. A map of the different regions as identified by the thresholds on enstrophy; v_L (solid lines) and v_I (dashed lines).

Although the exact values obtained by the two estimates differ, the trends are very consistent. As time progresses, the threshold level for which $v_n = 0$ moves to lower and lower levels, in accordance with the decay expected from self-similarity. The threshold level demarcating the beginning of the VSL remains approximately constant at $\omega_0^2/\omega_r^2 \approx 10^{-5}$ for $t/t^* > 150$.

Using these two threshold levels we can distinguish three regions: (i) the core region, where inviscid production, viscous transport and dissipation are all important; (ii) the intermediate region, which can be compared to the buffer layer of a wall-bounded turbulent flow in the sense that both viscous and inertial effects are important; and (iii) the VSL, which is dominated by viscous transport and dissipation. The results presented in Da Silva & Pereira (2008); Da Silva & Taveira (2010); Taveira & Da Silva (2013) are all obtained with threshold values corresponding to the core region. Note that, similar to the viscous sublayer in a wall-bounded flow, the VSL can neither be classified as turbulent because viscous effects are dominant nor as laminar because there are significant fluctuations in the layer due to external influences. Fig. 8 demonstrates how close the turbulent core region is to the VSL. The core region occupies most of the turbulent fluid and contains many "holes", whereas the VSL forms a thin strip in the white region immediately adjacent to the isoline marked as $|v_n^P/v_n| < 0.05$. The intermediate region is very thin, and seems to be thinner ahead of the turbulent events travelling from left to right on the figure, and thicker in their wakes.

4.3. Geometry

The dependence of volume V and surface area S on the threshold value ω_0^2 can be used to obtain information about the average distance from one enstrophy isosurface to the next, thereby getting an impression of the distance between different regions of the flow. The average distance n , the volume V_T for which $\omega^2 > \omega_0^2$ and the surface area S are

† The sum of V and V_T is exactly half of the simulation domain volume.

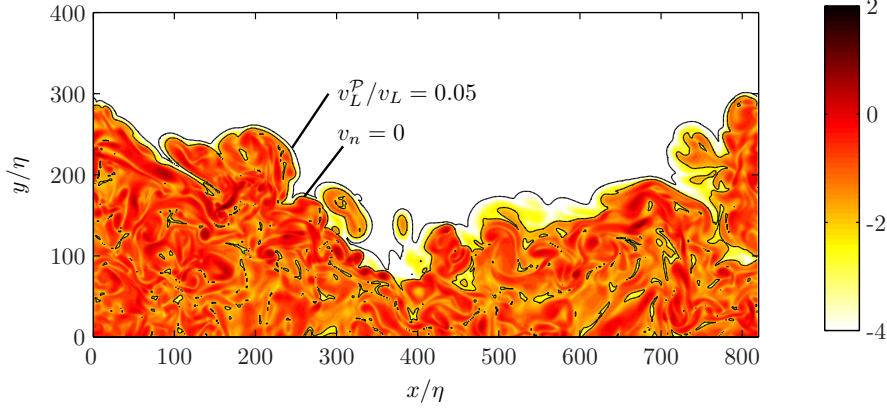


FIGURE 8. A field in cross-section showing $10 \log(\omega^2/\omega_r^2)$ at $t/t^* = 150$. Clearly visible is the close proximity of the core region to the VSL.

related by

$$\frac{dV_T}{dn} = S. \quad (4.2)$$

Introducing $\Delta V_T = V_{T;i+1} - V_{T;i}$ and $\Delta n = n_{i+1} - n_i$ as the difference in volume and distance respectively between two adjacent enstrophy thresholds $\omega_{0;i}^2$ and $\omega_{0;i+1}^2$, the average distance can be approximated by $\Delta n \approx 2\Delta V_T/(S_i + S_{i+1})$. We set $n = 0$ at the start of the VSL at $\omega_0^2/\omega_r^2 = 10^{-5}$.

The dependence of n on ω_0^2 is shown for $t/t^* > 150$ in Fig. 9(a). The collapse of the profiles for different times shows that the result is quite robust. It is striking how close essentially irrotational regions are located to regions with very high enstrophy levels on average. Indeed, the core region is on average about 10η away from the VSL. Moreover, the full 24 decades in enstrophy levels are separated by 25η . Also shown is the analytical solution (2.11) (dotted line), expressed as $\omega_0^2/\omega_r^2 = \exp(\alpha_\eta(n - n_r)/\eta)$ with $\alpha_\eta = 3.7$. It is evident that (2.11) is a reasonable approximation for $\omega_0^2/\omega_r^2 \ll 1$, which explains the agreement of the simulation data with the predictions for v^D and v^E . However, as can be seen, the shape of the n profile deviates from a straight line in a semilog plot because of the influence of surface area S on v_n . Indeed, the model assumes that v_n is constant and this has clearly shown to be not the case for this flow. Fig. 9(b) shows the normalized distance for a number of thresholds as a function time. After $t/t^* = 150$, the distances become nearly constant, indicating that the jet edge has reached a dynamic equilibrium and the distances between isosurfaces scale with η .

5. Concluding remarks

The results presented in this paper show convincing evidence for the existence of the VSL. Consistent with earlier work, we find that inertial processes are negligible in the VSL and that this layer is discernible for nearly twenty orders of magnitude in enstrophy threshold, a range corresponding to an average distance of 15η . The VSL was present for $\omega_0^2/\omega_r^2 < 10^{-5}$ and was practically independent of time for the duration of the simulation. The simple theoretical model derived in §2.3 is in good agreement with the data and shows that the contribution of the viscous transport term amount to $2v_n$ and the viscous destruction term to $-v_n$.

Whilst v_n was of the same order of magnitude as u_η , there was a clear dependence of the value of v_n on the enstrophy threshold. This suggests that Corrsin's dimensional

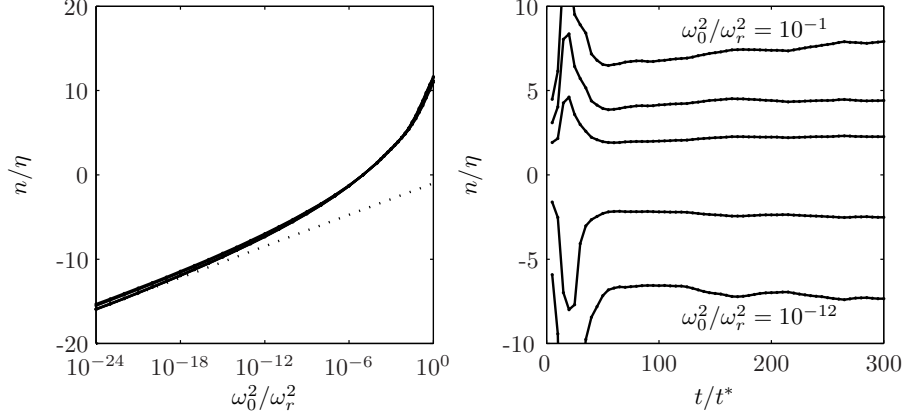


FIGURE 9. (a) thickness as a function of threshold value; b) thickness as a function of time.

arguments may not convey the entire story of the outer fringes of a turbulent zone. Indeed, we found that the classical inviscid entrainment assumption $u_e = \alpha \hat{u}$ best described the entrainment in the VSL as $Q_e = v_n S$ is practically independent of the threshold value. This implies that both viscous transport velocity and surface area adjust to the imposed global rate so that the outcome is independent of threshold. As the VSL becomes less contorted when moving out of the turbulent region v_n needs to become larger to maintain a constant entrainment flux. Note that the inviscid entrainment assumption works for the global behaviour, but the local physics of the VSL are all but inviscid and governed by viscous diffusion of enstrophy.

The small dependence on ω_0^2 that was observed when plotting u_e/\hat{u} could be explained by taking into account the average position $\langle y \rangle_S/b$ of the interface. Using that the VSL spans $\sim 15\eta$ and $b \approx 150\eta$ the expected difference is about 10% for the case considered here, which is consistent with Fig. 6(b). Employing Corrsin's assumption that the thickness of the VSL is $\sim \eta$ and noting that $b \sim \eta Re^{3/4}$, it follows that as Re tends to infinity, the ratio $\langle y \rangle_S/b \rightarrow$ will become constant throughout the VSL. Hence, this appears to be a low-Reynolds number correction.

Three regions were observed for the flow under consideration. For roughly $\omega_0^2/\omega_r^2 < 10^{-5}$, we observed the VSL which is characterised by a propagation velocity only depending on viscous processes. The core region was categorised as that region of the flow for which $v_n > 0$, i.e. regions that become smaller in time and that are responsible for the $\overline{\omega'\omega'} \propto t^{-2}$ behaviour. The enstrophy threshold at which this region was observed was a decreasing function of time. In between the VSL and the core region there was an intermediate region providing a smooth transition from one region to the other.

This study suggests that the reported differences in the thickness of the TNTI and the VSL are due to different choices of the threshold. Indeed, Da Silva & Pereira (2008); Da Silva & Taveira (2010); Taveira & Da Silva (2013) use a threshold value which is associated with the core region. The distance from the core region to the VSL is about 10η for the Re under consideration, which is a value not atypical to that mentioned in Da Silva & Pereira (2008). The fact that the core region is fully turbulent may provide an explanation for why the layer thickness is found to scale with the Taylor length scale λ . We should point out that another possible explanation for the difference might be that Da Silva & Pereira (2008) use conditional statistics that are dependent on the inhomogeneous direction only - and not along isosurfaces as was done in this paper.

Further work, particularly a study of the Re dependence is necessary to be able to make a firmer statement about the difference in boundary layer scaling.

Finally, it may be argued that the term turbulent-nonturbulent "interface" is slightly misleading, as it suggests (i) a surface separating two regions; and (ii) a sharp distinction between the character of the flow in these two regions. Consistent with earlier work, we find that the transition from turbulent to non-turbulent occurs over a thin but finite region, in which the flow changes smoothly from one region to another. Any particular threshold value to demarcate the turbulent/nonturbulent interface is then by definition construed. Furthermore, the current work suggests that the TNTI comprises both the intermediate region and the VSL, confirming the conjecture that the VSL is contained inside the TNTI region made by Bisset *et al.* (2002).

Acknowledgements

The computational resources for this work were provided by the Imperial College HPC facilities. Both authors benefited greatly from an inspiring MULTIFLOW workshop on the Turbulent/Non-turbulent Interface which took place in October 2012 in Madrid. M. H. acknowledges financial support from the Swiss National Science Foundation (SNF) under grant number PBEZP2-127831 and from the European Commission under the Marie Curie Intra-European Fellowship, project number 272886.

REFERENCES

- BISSET, D. K., HUNT, J. C. R. & ROGERS, M. M. 2002 The turbulent/non-turbulent interface bounding a far wake. *J. Fluid Mech.* **451**, 383–410.
- CORRSIN, S. & KISTLER, A. 1955 Free stream boundaries of turbulent flows. *Tech. Rep.* 1244. NACA.
- DA SILVA, C. B. & MÉTAIS, O. 2002 On the influence of coherent structures upon interscale interactions in turbulent plane jets. *J. Fluid Mech.* **473**, 103–145.
- DA SILVA, C. B. & PEREIRA, J. C. F. 2008 Invariants of the velocity-gradient, rate-of-strain, and rate-of-rotation tensors across the turbulent/nonturbulent interface in jets. *Phys. Fluids* **20** (5), 055101.
- DA SILVA, C. B. & TAVEIRA, R. P. 2010 The thickness of the turbulent/nonturbulent interface is equal to the radius of the large vorticity structures near the edge of the shear layer. *Phys. Fluids* **22** (5), 121702.
- HOLZNER, M., LIBERZON, A., NIKITIN, N., KINZELBACH, W. & TSINOBER, A. 2007 Small-scale aspects of flows in proximity of the turbulent/nonturbulent interface. *Phys. Fluids* **19** (7), 071702.
- HOLZNER, M., LIBERZON, A., NIKITIN, N., LUETHI, B., KINZELBACH, W. & TSINOBER, A. 2008 A Lagrangian investigation of the small-scale features of turbulent entrainment through particle tracking and direct numerical simulation. *J. Fluid Mech.* **598**, 465–475.
- HOLZNER, M. & LUETHI, B. 2011 Laminar superlayer at the turbulence boundary. *Phys. Rev. Lett.* **106** (13), 134503.
- HUNT, J. C. R., EAMES, I., DA SILVA, C. B. & WESTERWEEL, J. 2011 Interfaces and inhomogeneous turbulence. *Phil. Trans. R. Soc. A* **369**, 811–832.
- HYMAN, J. & SHASHKOV, M. 1997 Natural discretizations for the divergence, gradient, and curl on logically rectangular grids. *Comput. Math Appl.* **33**, 81–104.
- MORTON, B. R., TAYLOR, G. I. & TURNER, J. S. 1956 Turbulent gravitational convection from maintained and instantaneous sources. *Proc. R. Soc. Lond.* **234**, 1–23.
- PHILIP, J. & MARUSIC, I. 2012 Large-scale eddies and their role in entrainment in turbulent jets and wakes. *Phys. Fluids* **24**, 055108.
- POPE, S. B. 2000 *Turbulent flows*. Cambridge University Press.
- REDFORD, J. A., CASTRO, I. P. & COLEMAN, G. N. 2012 On the universality of turbulent axisymmetric wakes. *J. Fluid Mech.* **710**, 419–452.

- VAN REEUWIJK, M. 2011 A mimetic mass, momentum and energy conserving discretization for the shallow water equations. *Comp. Fluids* **46**, 411416.
- VAN REEUWIJK, M., JONKER, H. J. J. & HANJALIĆ, K. 2008 Wind and boundary layers in Rayleigh-Bénard convection. i. analysis and modelling. *Phys. Rev. E* **77**, 036311.
- SREENIVASAN, K. R., RAMSHANKAR, R. & MENEVEAU, C. 1989 Mixing, entrainment and fractal dimensions of surfaces in turbulent flows. *Proceedings of the Royal Society of London Series A-mathematical Physical and Engineering Sciences* **421** (1860), 79–&.
- STULL 1998 *An introduction to boundary layer meteorology*. Kluwer Academic Publishers.
- TAVEIRA, R. P. & DA SILVA, C. B. 2013 Kinetic energy budgets near the turbulent/nonturbulent interface in jets. *Phys. Fluids* **25**, 015114.
- TENNEKES, H. & LUMLEY, J. L. 1972 *A First course in Turbulence*. MIT Press.
- THORPE, S. A. 2005 *The turbulent ocean*. Cambridge University Press.
- TOWNSEND, A. A. 1976 *The structure of turbulent shear flow*. Cambridge University Press.
- TRITTON, D. J. 1988 *Physical fluid dynamics*. Calendon, Oxford.
- TURNER, J. S. 1986 Turbulent entrainment: the development of the entrainment assumption, and its application to geophysical flows. *J. Fluid Mech.* **173**, 431–471.
- VERSTAPPEN, R. W. C. P. & VELDMAN, A. E. P. 2003 Symmetry-preserving discretization of turbulent flow. *J. Comput. Phys.* **187** (1), 343–368.
- WESTERWEEL, J., FUKUSHIMA, C., PEDERSEN, J. M. & HUNT, J. C. R. 2005 Mechanics of the turbulent-nonturbulent interface of a jet. *Phys. Rev. Lett.* **95** (17), 174501.
- WESTERWEEL, J., FUKUSHIMA, C., PEDERSEN, J. M. & HUNT, J. C. R. 2009 Momentum and scalar transport at the turbulent/non-turbulent interface of a jet. *J. Fluid Mech.* **631**, 199–230.
- WOLF, M., LÜTHI, B., HOLZNER, M., KRUG, D., KINZELBACH, W. & TSINOBER, A. 2012 Investigations on the local entrainment velocity in a turbulent jet. *Phys. Fluids* **24** (10), Attached publisher’s note: Erratum: ‘Investigations on the local entrainment velocity in a turbulent jet’ [Phys. Fluids 24, 105110 (2012)], Phys. Fluids 25, 019901 (2013).